The Abdus Salam
International Centre for Theoretical Physics

United Nations
Educational, Scientific
and Cultural Organization

International Atomic
Energy Agency

SMR 1673/53

AUTUMN COLLEGE ON PLASMA PHYSICS

5 - 30 September 2005

Shear-driven fluctuations in magnetized plasma: theory and lab comparisons PART I

M. KOEPKE

Physics Dept., West Virginia University,
Morgantown, USA

Shear-driven fluctuations in magnetized plasma: Theory and lab comparisons

Mark Koepke
Physics Dept., West Virginia University, Morgantown, WV 26506 USA
work supported by U.S. National Science Foundation

Useful discussions with V. Gavrishchaka, G. Ganguli, W. Amatucci, J. Carroll, C. Teodorescu, E. Reynolds, R. Hatakeyama, T. Kaneko, E. Scime, & R. Merlino are gratefully acknowledged.

- Shear in the ion perpendicular drift velocity
- Shear in the ion parallel drift velocity
- Ion-cyclotron instability
- Ion-acoustic instability
- Universal (density-gradient drift) instability

Outline

- Overview of shear-driven effects
  - Dissipative and reactive responses
- Physics of shear in the ion perpendicular flow
- Physics of shear in the ion parallel flow
- Overview of laboratory observations
- Ion-cyclotron instability
- Ion-acoustic instability
- Universal (density-gradient drift) instability
- Conclusions, so far, of the ongoing exploration

Shear-driven fluctuations span wide range of frequency and wavelength

- Zero-frequency, large wavelength
  - perpendicular and parallel Kelvin-Helmholtz waves
- Ion-acoustic and diamagnetic-drift frequencies
  - inhomogeneous energy-density driven waves
  - parallel-flow shear driven waves
- Ion-cyclotron frequency, medium wavelength
  - inhomogeneous energy-density driven waves
  - parallel-flow shear driven waves
- Lower-hybrid frequency, small wavelength
  - electron-ion hybrid waves

Conceptual description of shear effects

- Regions I and II have relative drift velocity (perpendicular or parallel to the magnetic field)
- Rate of region I wave-energy increase: contribution from region I wave-particle interactions minus region I energy lost to region II because of outward wave propagation (wave-wave interaction)
- If regions I and II have waves with opposite sign of energy density, this last contribution will cause region I wave growth

Velocity Distribution in Shear Layer

$$f_{0\perp} = \beta \exp\left[-\frac{\beta}{2}\left(v_x^2 + \frac{\left[v_y - V_E(x)\right]^2}{\eta(x)}\right)\right]$$

$\beta = 1/v_{thi}^2$
$V_E = -E(x)/B$
$\eta(x) = (1+V_E'(x)/\Omega)$
$v_{thi}^2 = k_B T_i / m_i$
m_i is the ion mass
k_B is Boltzmann's constant
Ω is the ion cyclotron frequency
the prime denotes differentiation with respect to x.

The simulation was run for 5 different ion masses applicable to Q-machines

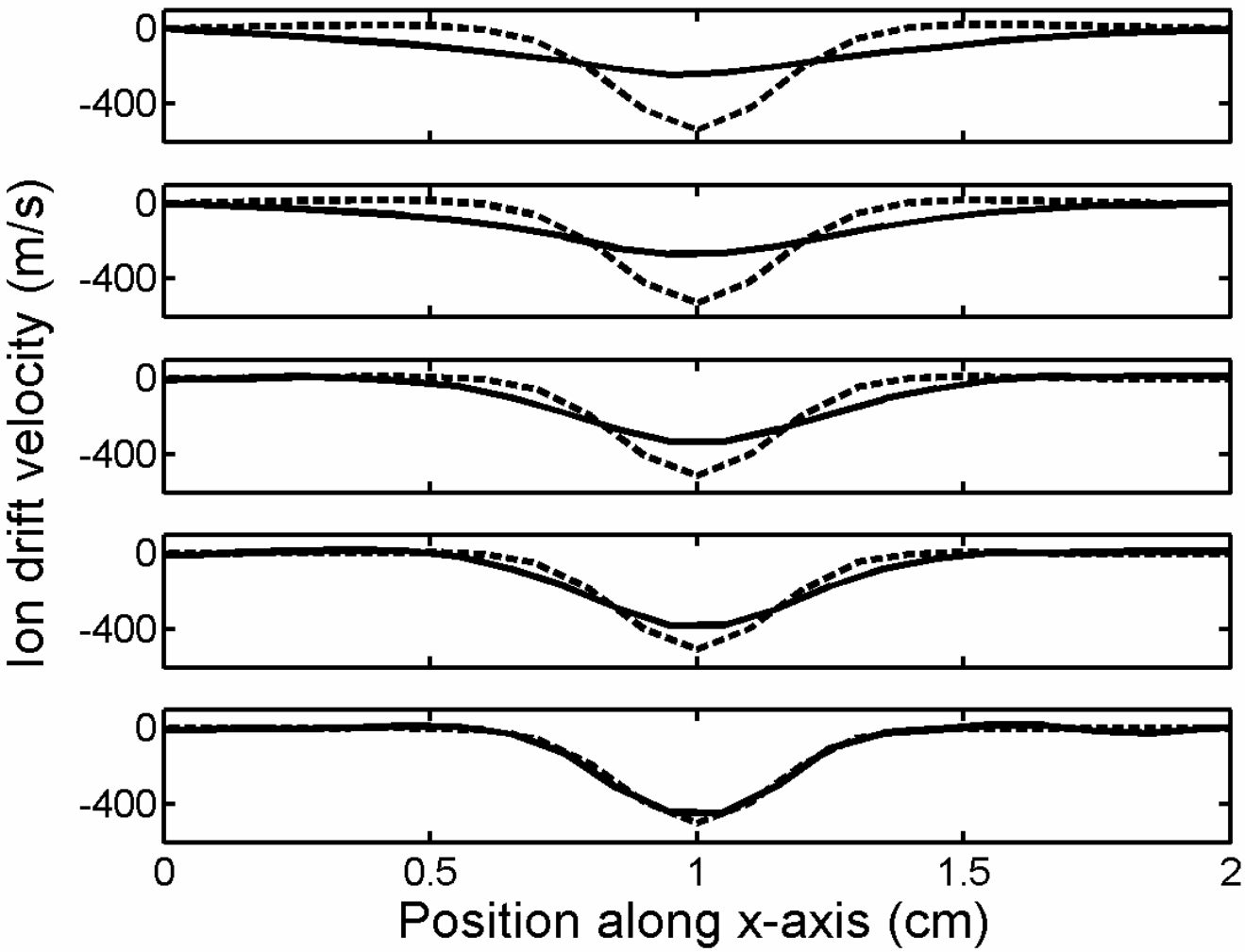

The simulation was run for Li, Na, K, Rb, and Ba. The physical parameters were E_{max}=100 V/m, B=0.2 Tesla and a=0.2 cm. This covers a range in epsilon from 0.36 to 1.60. The solid line is the simulation result while the dashed line is the ***E***x***B*** fluid calculation. The electric-field profile is represented by Gaussian profiles centered around +-1.0 cm.

The maximum ion-drift is reduced by finite-Larmor-radius effects

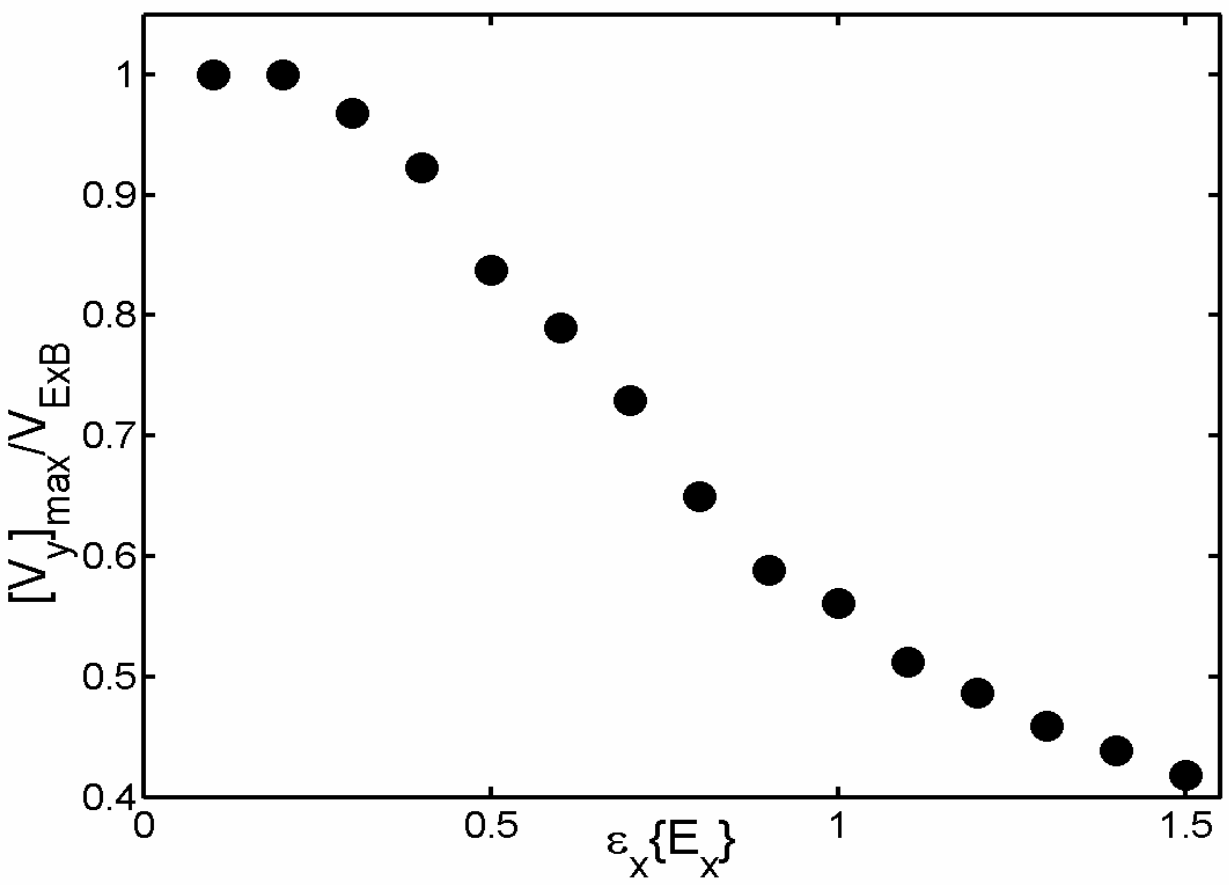

For this figure the simulation was run for increasing ion temperature such that only $\varepsilon_x\{E_x\}$ was changed. The maximum drift is approximately halved when the gyro-diameter equals the layer width. This has the effect of reducing the maximum shear to 50% of that which one would infer from the electric-field profile.

The width of the ion-drift profile is increased by finite-Larmor-radius effects

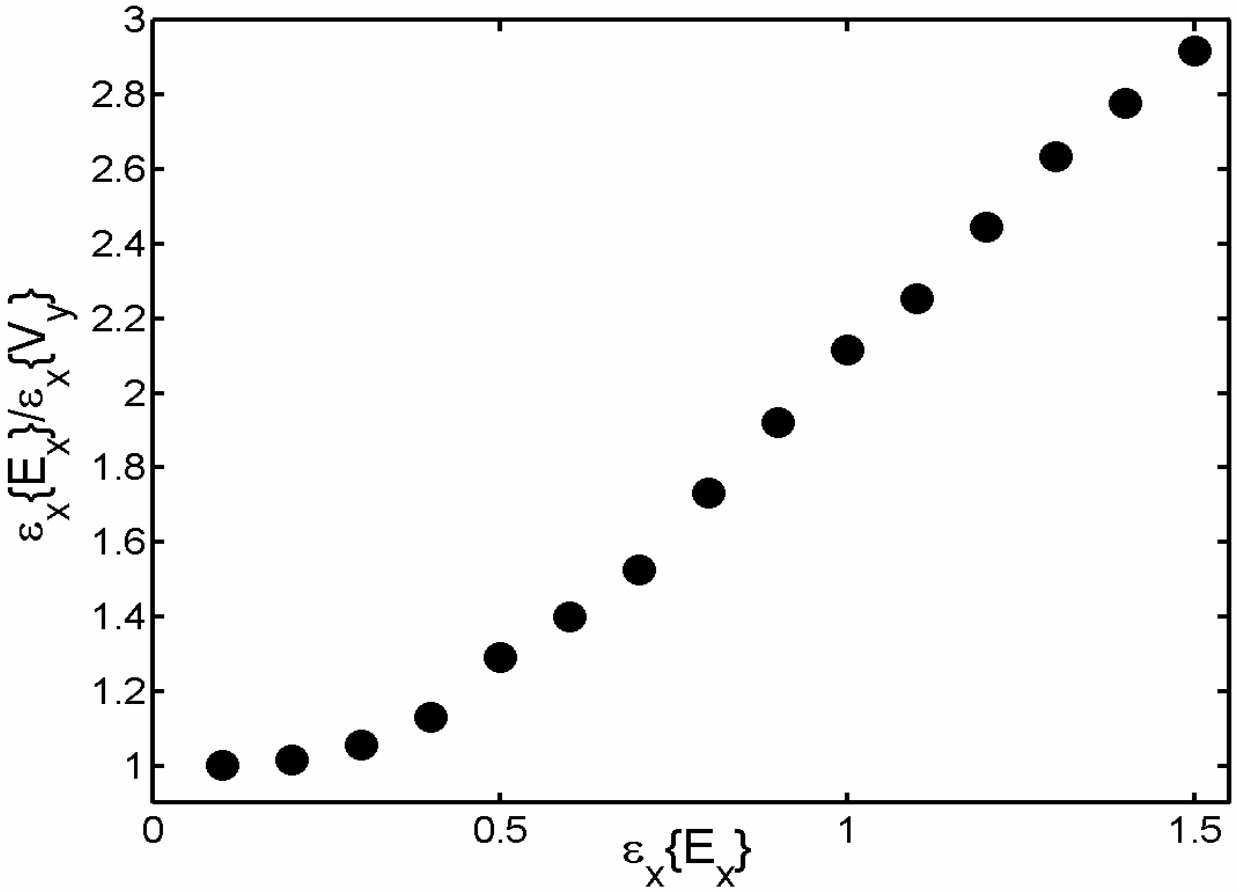

This figure was made from the same simulation runs as in the last slide. The layer width is approximately doubled when the gyro-diameter equals the layer width. This, coupled with the reduced drift magnitude, has the effect of reducing the maximum shear to ~25% of that which one would infer from the electric-field profile.

Ion density reduction in regions of higher electric potential is due to ion finite-Larmor-radius trajectories

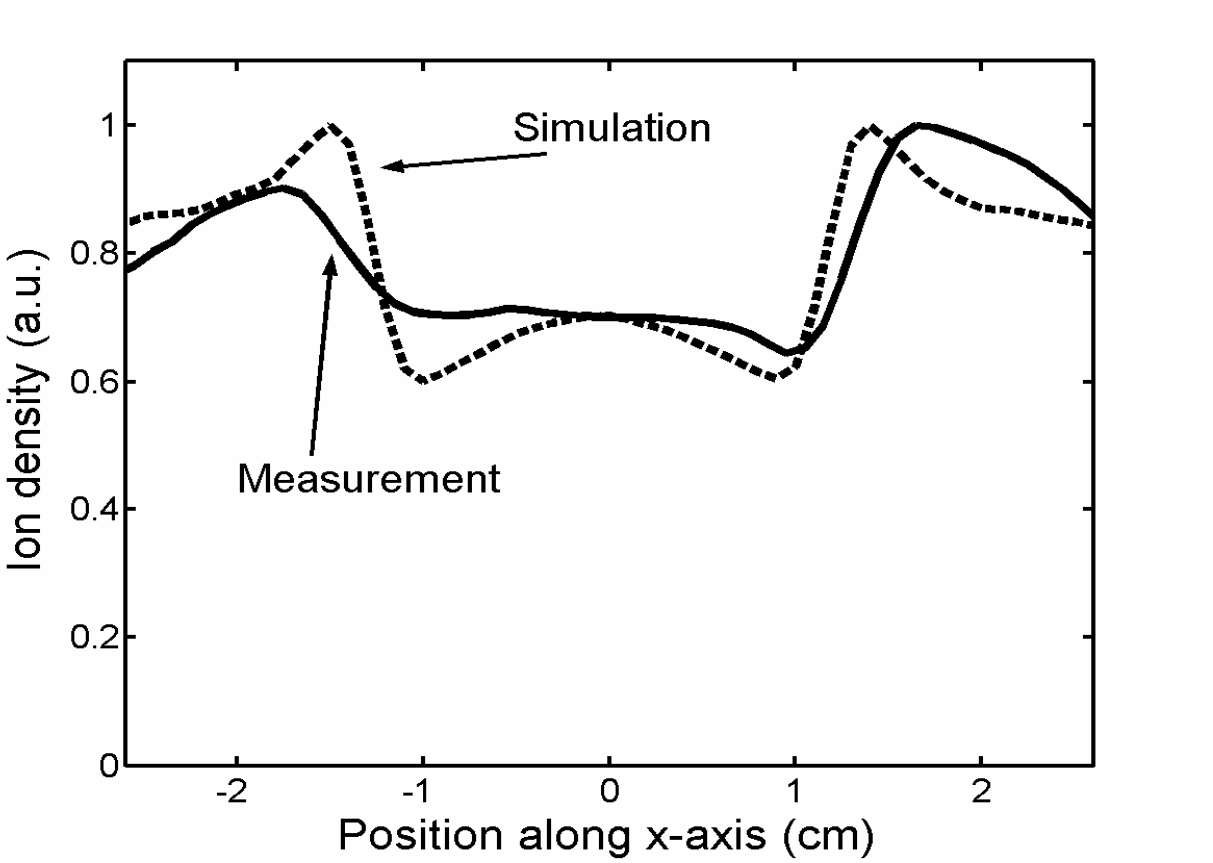

The simulation reproduces the observed density depletion. The simulation overestimates density gradients due to the exclusion of ion-ion collisions in the simulation. For the parameters of this experiment with Ba^+ plasma the collision frequency is ~0.1 ω_{ci}. This would cause some relaxation of the ion density gradients.

Experimental approach

- Generate localized radial electric field at interface of two co-axially separated plasma populations by applying a differential bias between the two plasma sources (hotplates).
- Measure the ion perpendicular-velocity distribution function using LIF for many values of $\varepsilon_x\{E_x\}$.
- Develop a test-particle simulation for calculating the ion perpendicular-velocity distribution function for arbitrary $\varepsilon_x\{E_x\}$.
- Validate the test-particle simulation by comparison with LIF measurements. Once validated, the simulation can be used to predict the ion-drift profile for ion species inaccessible to LIF diagnostics.

Q-machine with two plasma sources and two electrodes creates co-axial plasma populations

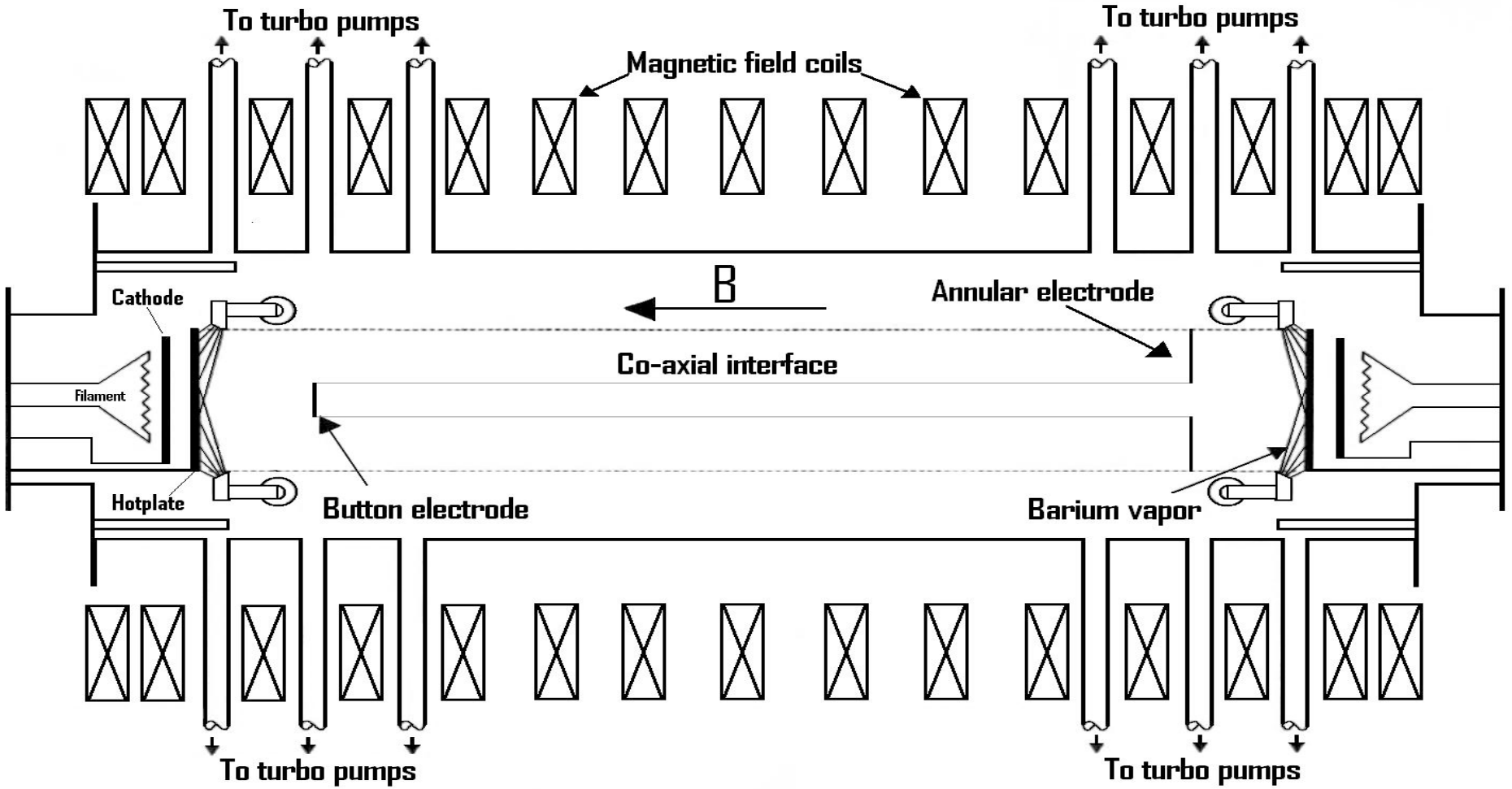

Perpendicular LIF diagnostic measures the ion velocity distribution f(V_y,x,y)

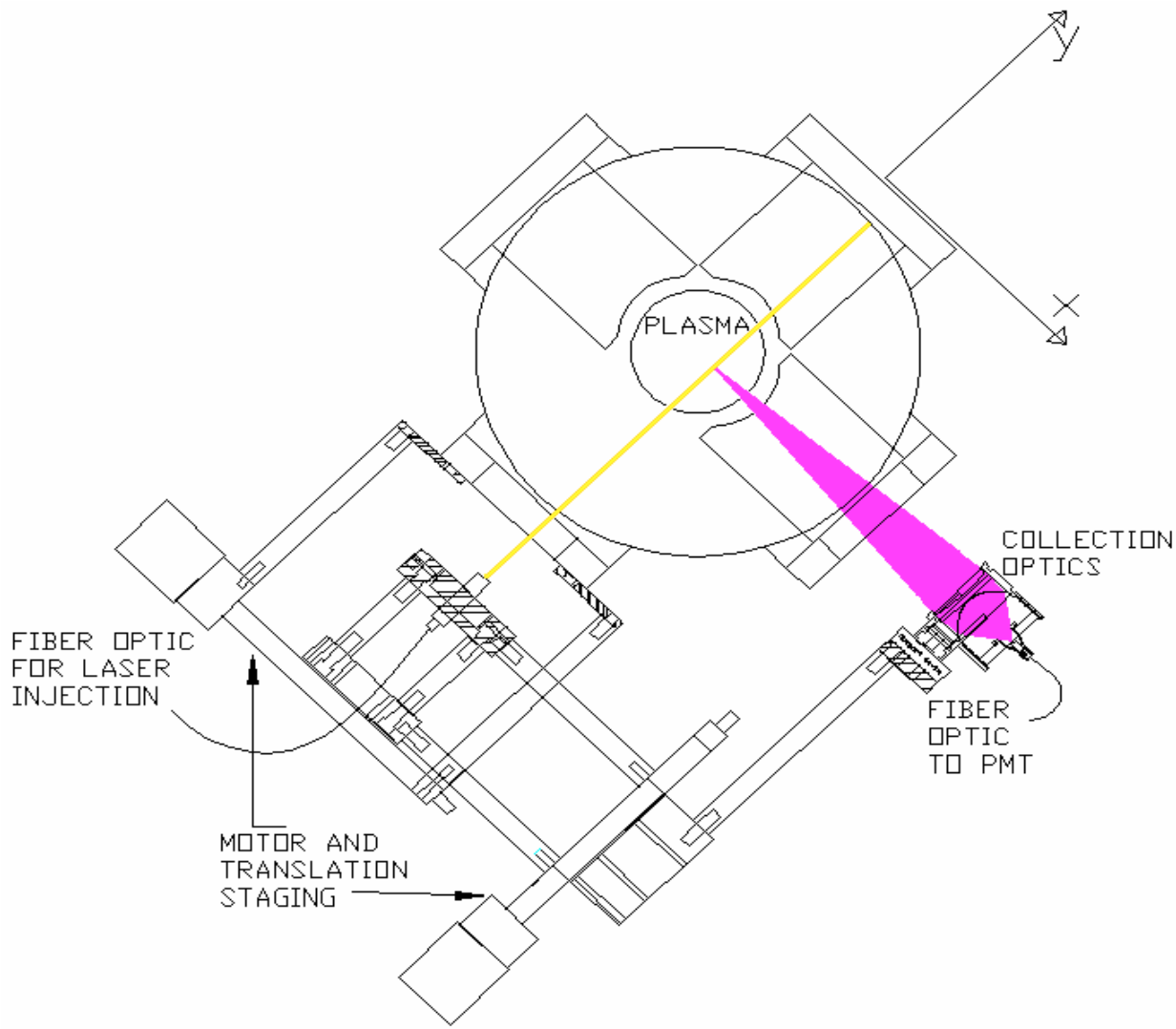

Optics for perpendicular LIF reduce the number of observed fluorescent transitions from ten to two

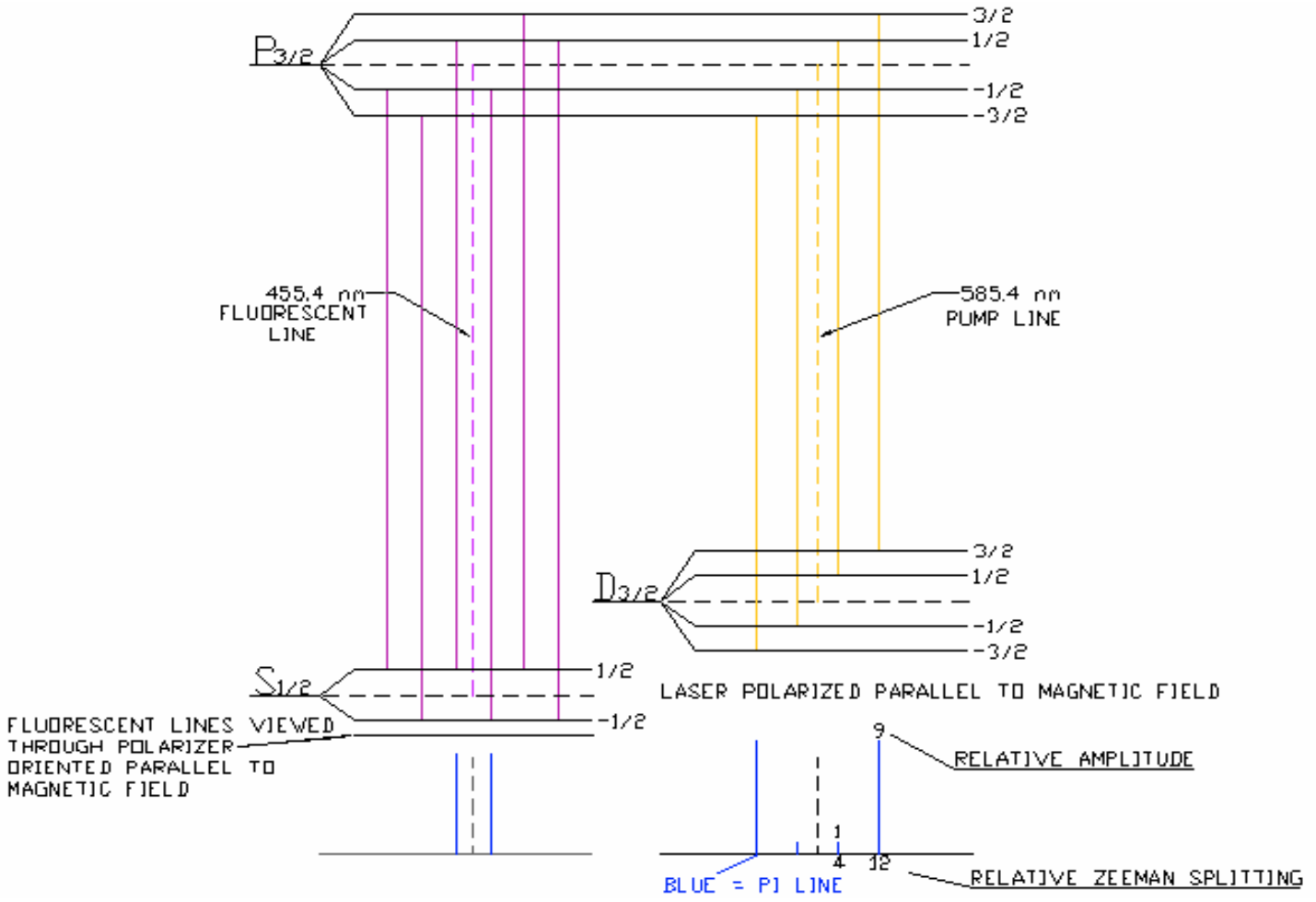

An Appropriately Zeeman Split Gaussian is fit to the LIF lineshape

LIF signal (dots) and its' full predicted Zeeman-split lineshape based on the fitted distribution function (solid line)

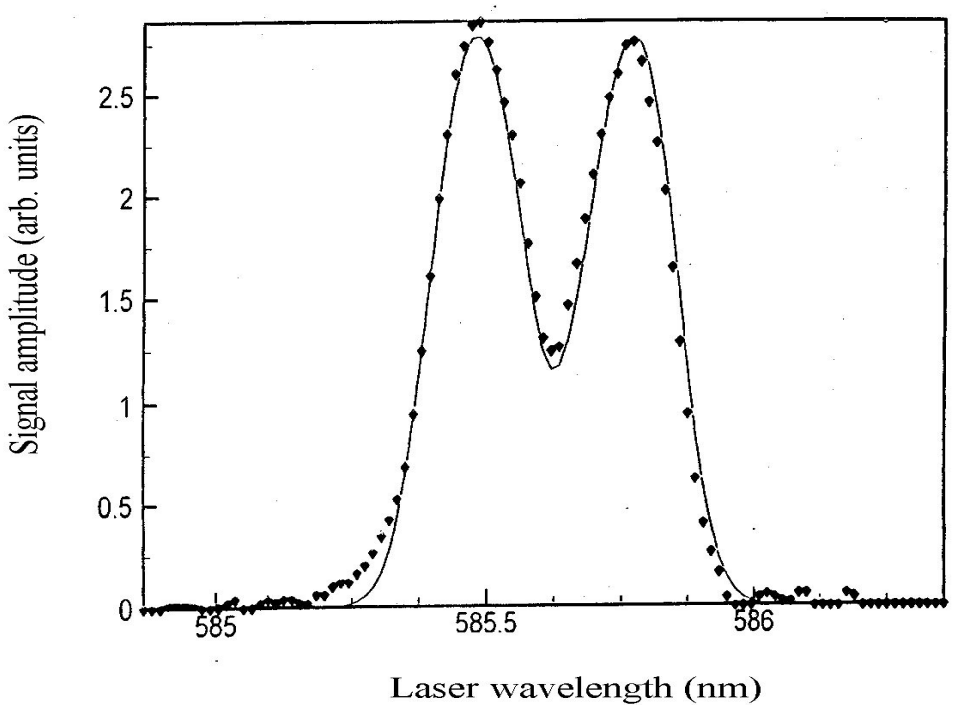

Best-fitted Maxwellian ion distribution function without Zeeman-splitting

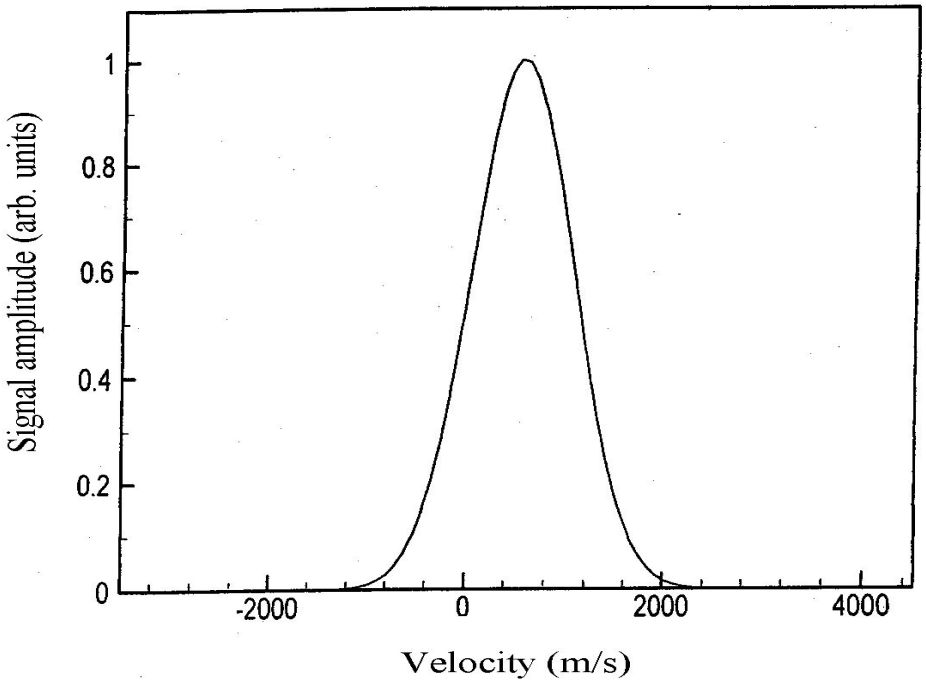

A large differential bias between the two plasma sources generates large electric fields at the interface

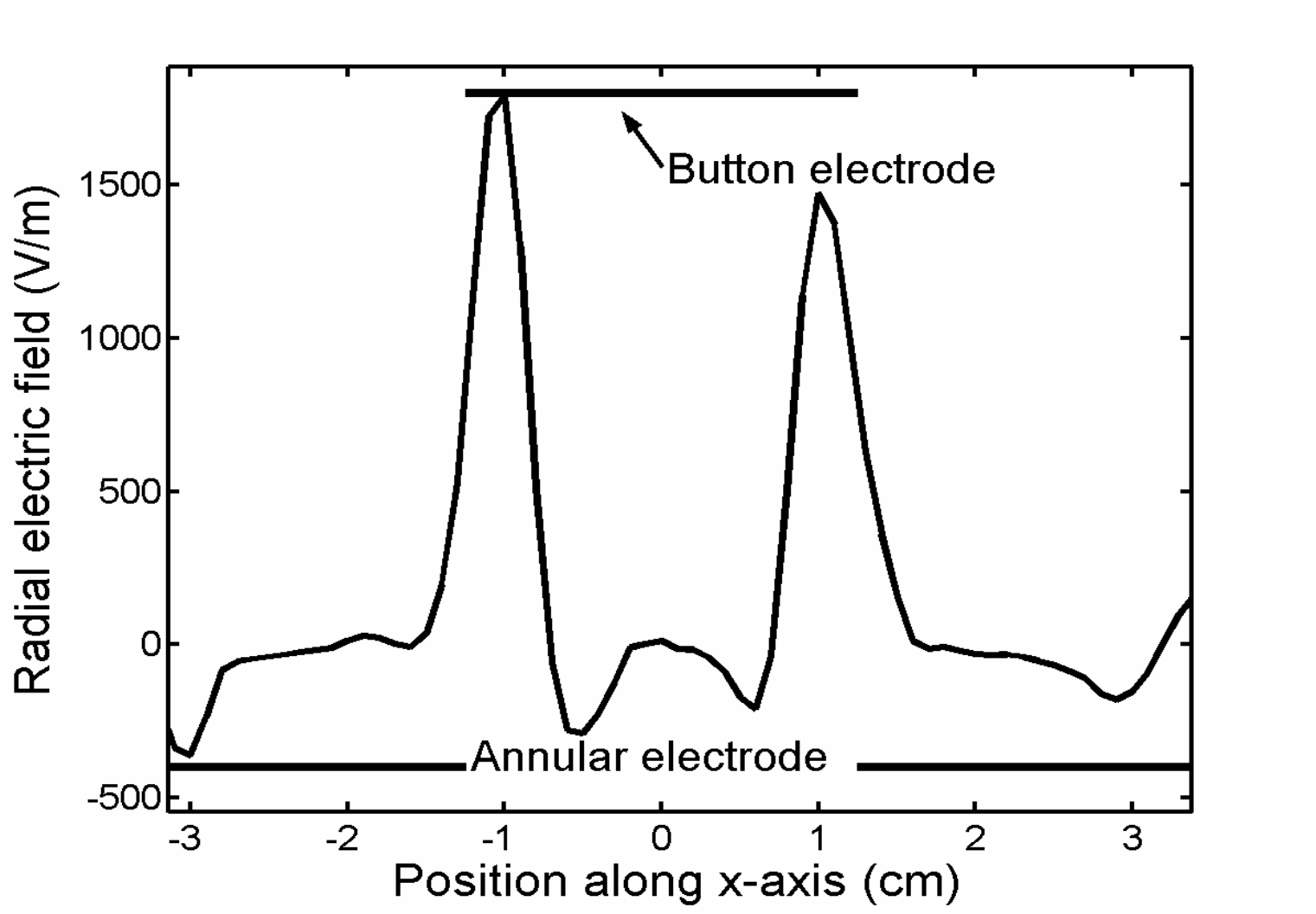

The electric-field inhomogeneity is characterized by the half-width at half-max of the electric-field profile

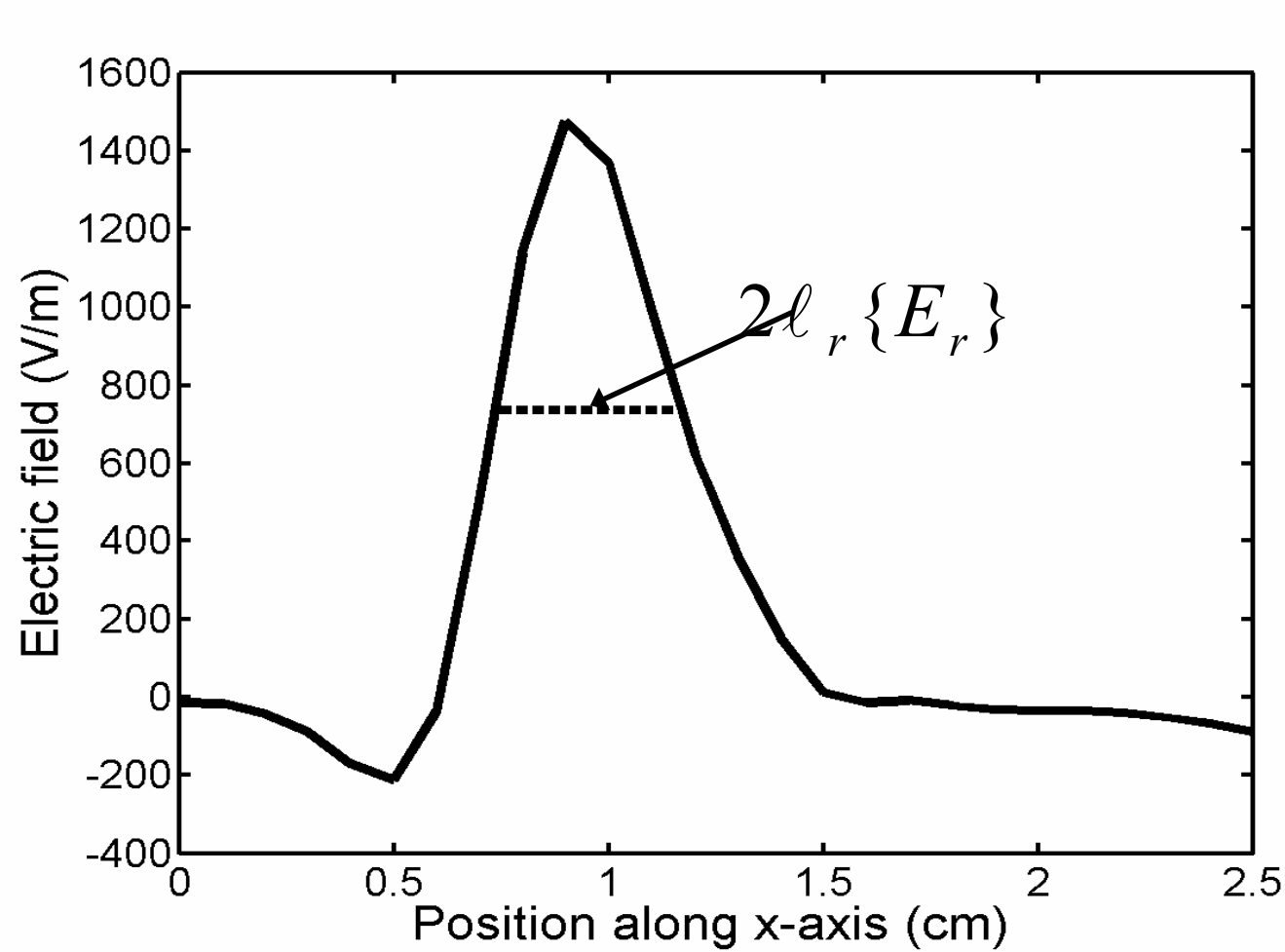

The large, localized electric field significantly modifies the ion-density profile

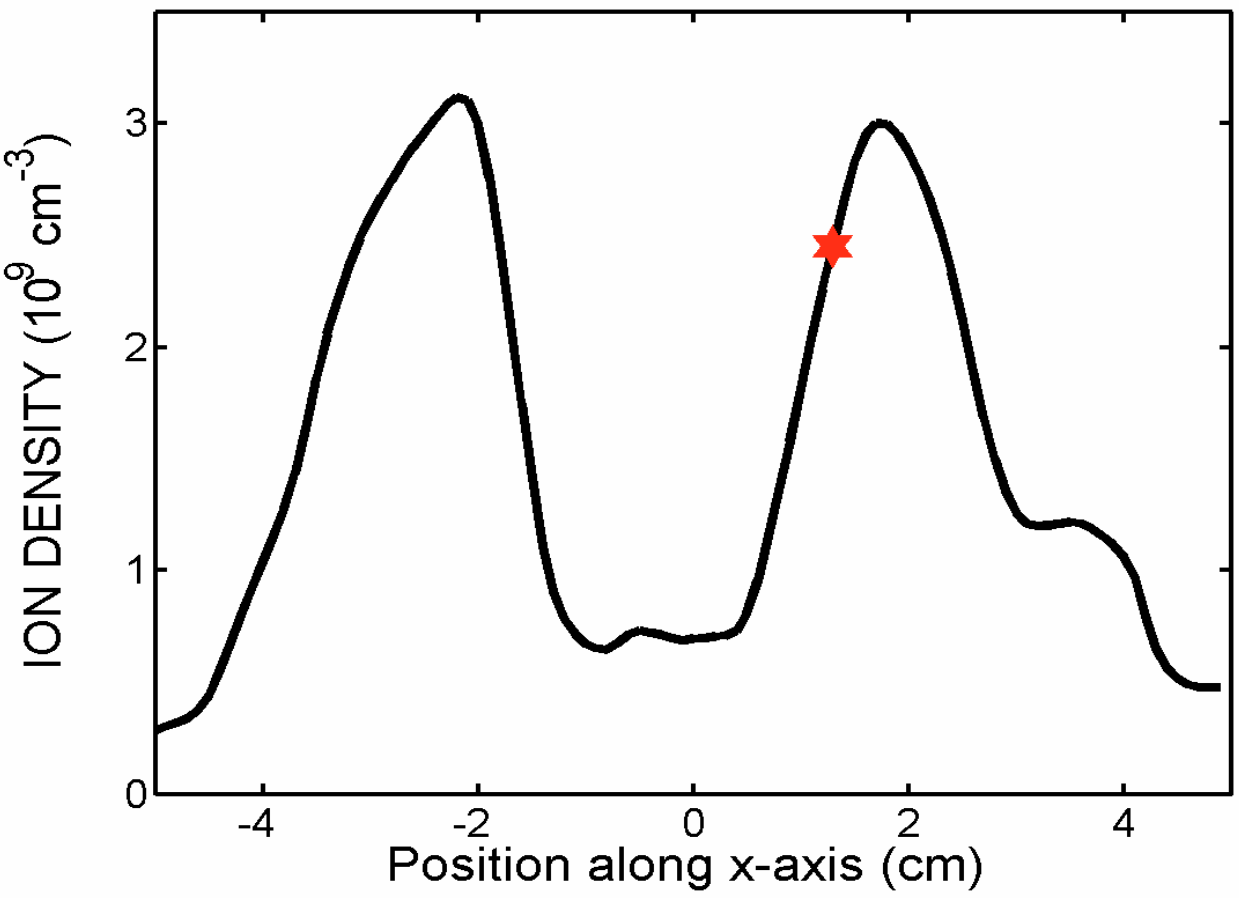

Fluid calculations of ion-drift profile based on the measured density and electric-field profiles show disagreement with LIF measurement (case with E_{max}=150 V/m)

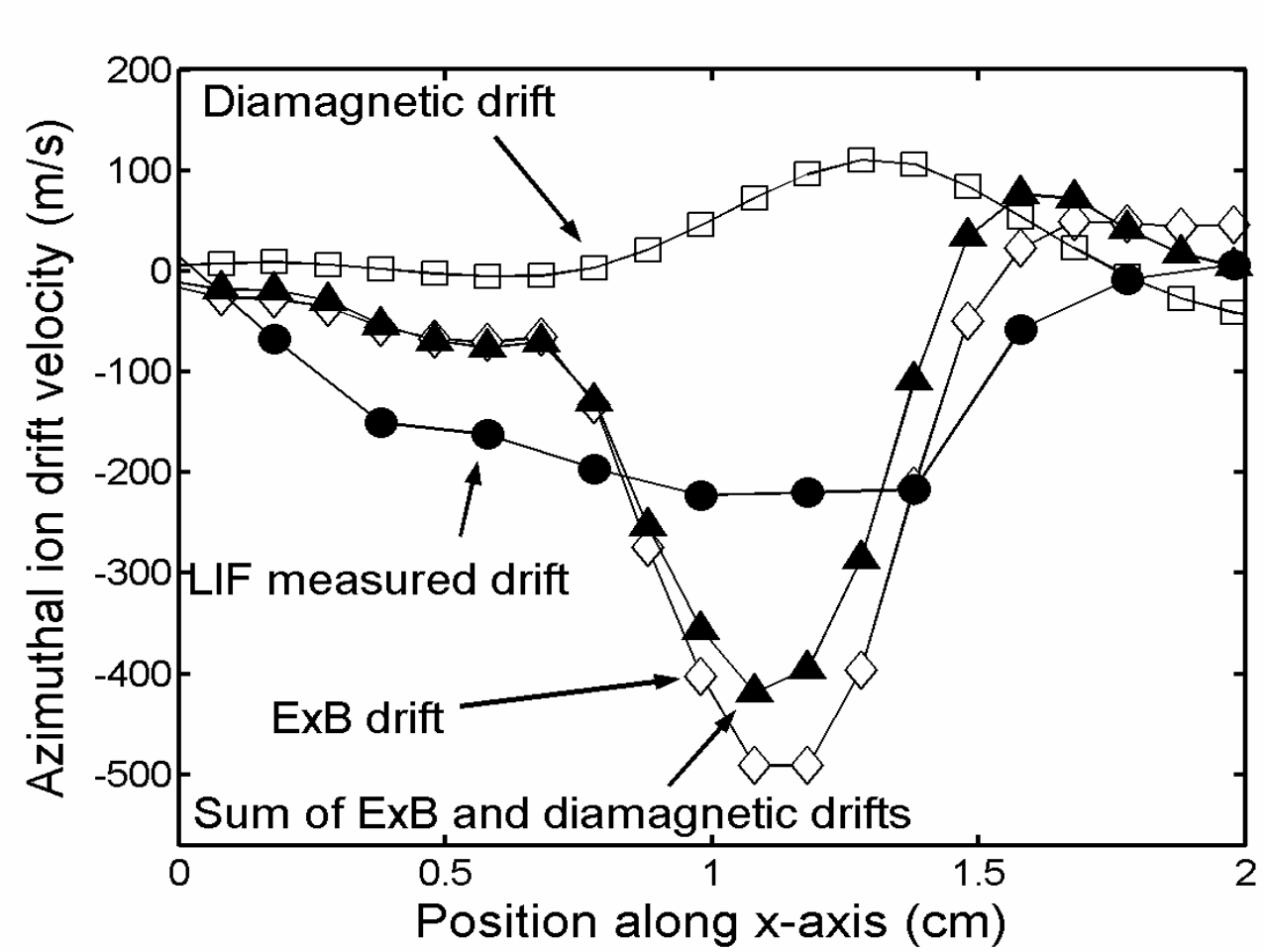

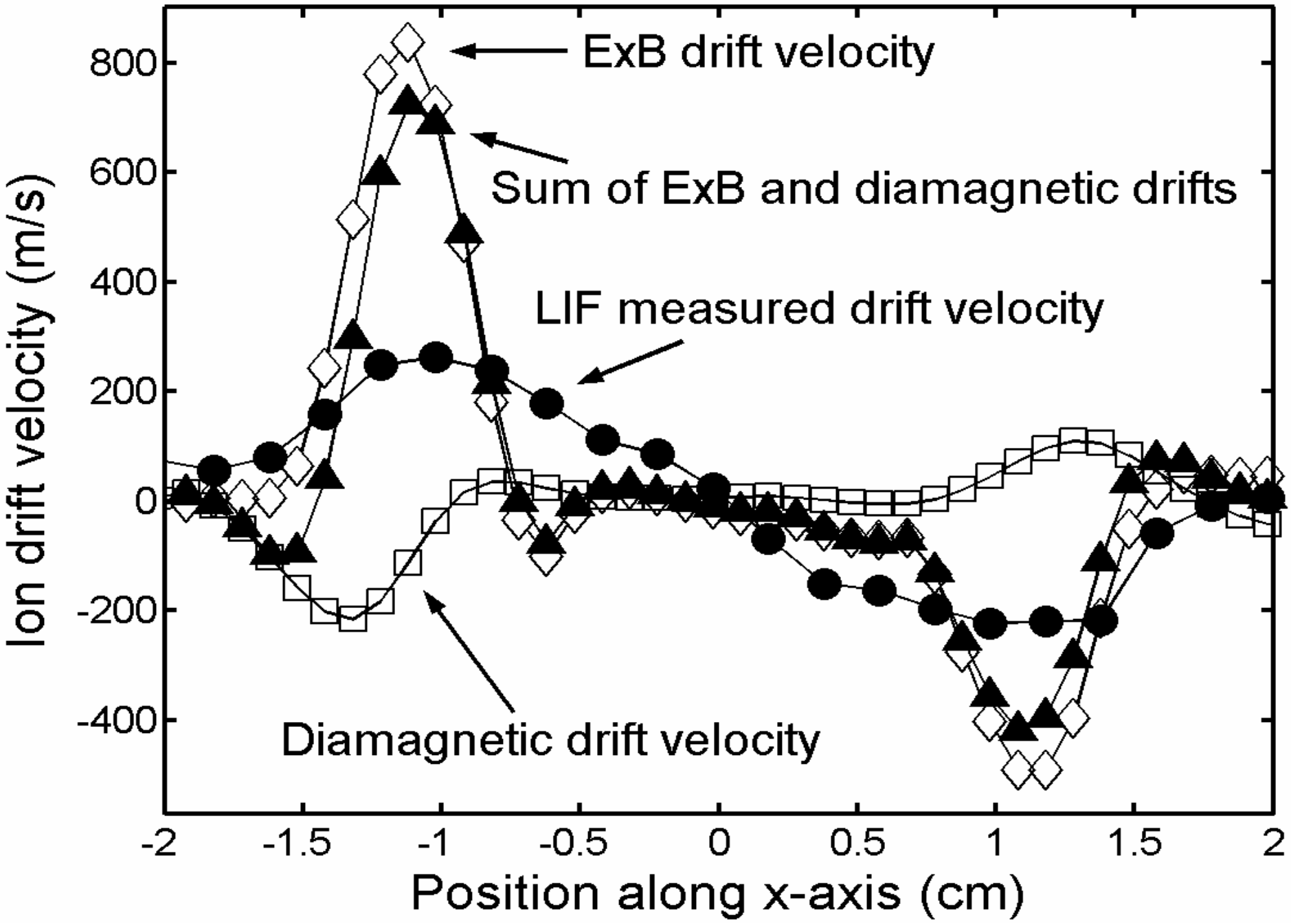
ExB drift velocity
Sum of ExB and diamagnetic drifts
LIF measured drift velocity
Diamagnetic drift velocity
Ion drift velocity (m/s)
Position along x-axis (cm)
800
600
400
200
0
-200
-400
-2
-1.5
-1
-0.5
0
0.5
1
1.5
2

Primary characteristics of shear-driven waves can be categorized by freq. and $k_\theta\rho_i$

Perp.-velocity shear	ω_R	$k_\theta\rho_i$	dv_θ/dr
DRIFT	$\omega_e^* \pm k_\theta v_E$	0.15 – 0.3	$< \omega_e^*$
ION-CYCLOTRON	$\omega_{ci} \pm k_\theta v_E$	0.4 – 1.5	$< \omega_{ci}$
LOWER-HYBRID	$\omega_{LH} \pm k_\theta v_E$	1.8 – 4	$> \omega_{LH}$

Parallel-velocity shear	ω_R	$k_\theta\rho_i$
DRIFT	$\omega_e^*/2 + \sqrt{[(\omega_e^*/2)^2 + (\sigma_0 k_z c_s)^2]}$	0.3
ION-ACOUSTIC	$\sqrt{[(\sigma_0 k_z c_s)^2]}$	0.5
ION-CYCLOTRON	$n\omega_{ci} + \sqrt[3]{[(\sigma_n k_z v_{thi})^2 n\omega_{ci}(T_e/T_i)\Gamma_n]}$	1 – 1.5

$$\sigma_n^2 \equiv 1 - \frac{k_y}{k_z}\frac{dv_{diz}/dx}{\omega_{ci}}\left(1 - \frac{n\omega_{ci}}{\omega}\right)$$

Theoretical Approach

- Sheared-velocity ion beam in background plasma was treated by *Lakhina* (*JGR* 1987). This treatment is for shear in the magnetic-field-aligned flow.
- General kinetic model for low-frequency electrostatic waves in inhomogeneous, magnetized plasma [*Ganguli et al*., 1989a; 1989b; 1994] includes a uniform magnetic field (positive z direction) and inhomogeneity $n(x)$, $v_{di}(x)$ and $v_{de}(x)$, $v_{Ei}(x)$, and $v_{Ee}(x)$. Shear in perp. and parallel ion flow.
- The restrictions $dv_{E\alpha}/dx > -\omega_{c\alpha}$ and $dn_{0\alpha}(x)/dx << n_{0\alpha}(x)/\rho_{\alpha}$ are required to obtain initial distribution functions that include the effects of perpendicular-velocity shear and, thus, are appropriate for deriving the general eigenvalue condition in the form of an integro-differential equation.
- An additional simplification is possible if the perpendicular-velocity shear is small $|dv_{E\alpha}/dx| << \omega_{c\alpha}$ and terms of (d^4/dx^4) and higher can be neglectable, in which case this integro-differential equation reduces to the second-order differential equation

Velocity Distribution in Shear Layer

$$f_{0\perp} = \beta \exp\left[-\frac{\beta}{2}\left(v_x^2 + \frac{\left[v_y - V_E(x)\right]^2}{\eta(x)}\right)\right]$$

$\beta = 1/v_{thi}^2$
$V_E = -E(x)/B$
$\eta(x) = (1+V_E'(x)/\Omega)$
$v_{thi}^2 = k_B T_i / m_i$
m_i is the ion mass
k_B is Boltzmann's constant
Ω is the ion cyclotron frequency
the prime denotes differentiation with respect to x.

Primary characteristics of shear-driven waves can be categorized by freq. and $k_\theta\rho_i$

Perp.-velocity shear	ω_R	$k_\theta\rho_i$	dv_θ/dr
DRIFT	$\omega_e^* \pm k_\theta v_E$	0.15 – 0.3	$< \omega_e^*$
ION-CYCLOTRON	$\omega_{ci} \pm k_\theta v_E$	0.4 – 1.5	$< \omega_{ci}$
LOWER-HYBRID	$\omega_{LH} \pm k_\theta v_E$	1.8 – 4	$> \omega_{LH}$

Parallel-velocity shear	ω_R	$k_\theta\rho_i$
DRIFT	$\omega_e^*/2 + \sqrt{[(\omega_e^*/2)^2 + (\sigma_0 k_z c_s)^2]}$	0.3
ION-ACOUSTIC	$\sqrt{[(\sigma_0 k_z c_s)^2]}$	0.5
ION-CYCLOTRON	$n\omega_{ci} + \sqrt[3]{[(\sigma_n k_z v_{thi})^2 n\omega_{ci}(T_e/T_i)\Gamma_n]}$	1 – 1.5

$$\sigma_n^2 \equiv 1 - \frac{k_y}{k_z}\frac{dv_{diz}/dx}{\omega_{ci}}\left(1 - \frac{n\omega_{ci}}{\omega}\right)$$

Dispersion Relation with Sheared Ion Flow

Ion-acoustic waves ($u \equiv k_z/k_y$):

$$\sum_{n=-\infty}^{\infty}\left[\frac{\omega_1}{\sqrt{2k_z^2v_{ti}^2}}Z\left\{\frac{\omega_1-n\omega_{ci}}{\sqrt{2k_z^2v_{ti}^2}}\right\}+\frac{dv_{di}/dx}{2u\omega_{ci}}Z'\left\{\frac{\omega_1-n\omega_{ci}}{\sqrt{2k_z^2v_{ti}^2}}\right\}\right]\Gamma_n(b_i)+\tau(1+F_{0e})+1+k^2\lambda_{Di}^2=0$$

$$\sigma_i^2+\sigma_e^2\frac{T_i}{T_e}+\sigma_i^2\frac{\omega-k_zv_{di}}{\sqrt{2k_z^2v_{ti}^2}}Z\left\{\frac{\omega-k_zv_{di}}{\sqrt{2k_z^2v_{ti}^2}}\right\}+\sigma_e^2\frac{T_i}{T_e}\frac{\omega-k_zv_{de}}{\sqrt{2k_z^2v_{te}^2}}Z\left\{\frac{\omega-k_zv_{de}}{\sqrt{2k_z^2v_{te}^2}}\right\}=0$$

where $\sigma_i^2 \equiv 1-(dv_{di}/dx)/(u\omega_{ci})$ and $\sigma_e^2 \equiv 1+(dv_{de}/dx)/(u\omega_{ce})$.

Ion-cyclotron waves:

$$\sum_{n=-\infty}^{\infty}\Gamma_n(b_i)\left[\left(\zeta_0+\frac{k_ydv_{di}/dx}{k_z\omega_{ci}}\right)\mathrm{Im}\,Z\{\zeta_{ni}\}\right]+\tau\left(1+\frac{k_ydv_{de}/dx}{k_z\omega_{ce}}\right)\mathrm{Im}\,Z\{\zeta_{0e}\}=0$$

$$\gamma/\omega_{ci}\propto\frac{\tau^{3/2}}{\mu^{1/2}}\left(\frac{k_zv_{de}}{\omega_{1r}}-1\right)-\sum_{n=-\infty}^{\infty}\Gamma_n(b_i)\left[1-\frac{dv_{di}/dx}{u\omega_{ci}}\left(1-\frac{n\omega_{ci}}{\omega_{1r}}\right)\right]\exp\left(-\frac{(\omega_{1r}-n\omega_{ci})^2}{2k_{\|}^2v_{ti}^2}\right)$$

Perpendicular-Velocity Shear

- The perpendicular electric field was found to be responsible for:
- a decrease in the threshold current for wave excitation, an increase in the azimuthal wave-vector component
- a discontinuity in real frequency
- an increase in the oscillation amplitude.
- Measurements of the linear properties of the mode verified the predictions from Ganguli's model and motivated detailed investigations of the model to significantly extend the range, detail, and interpretation of its predictions.

Parallel-Velocity Shear

- The consequence of a spatially varying parallel drift speed was investigated theoretically for cases of sharply [*Chandrasekhar*, 1961] and smoothly [*D'Angelo*, 1965] inhomogeneous velocity profiles.
- *D'Angelo* [1965] predicted a purely growing, electrostatic, ion instability driven by parallel-velocity shear. This has been termed the parallel Kelvin-Helmholtz instability [*Luo et al*., 2001], the parallel-velocity-shear instability [*Sen and Cairns,* 2000], and the D'Angelo mode [*Gavrishchaka et al*., 1998].
- We measure frequency in the lab frame ω_{lab}, whereas, in the drifting ion frame, the frequency ω_1 is equivalent to $\omega_{lab} - k_z v_{di}$. Using ω_1, we can obtain the wave phase velocity $v_{\phi z}$ ($=\omega_{1r}/k_z$) and compare $v_{\phi z}$ to velocities associated with positive and negative slope in the particle velocity distribution function.
- Conceptually, introducing parallel-velocity shear causes a diagmagnetic drift similar to that caused by a density gradient [*Gavrishchaka et al*., 1998].
- *Smith and von Goeler* [1968] express the shear-induced, off-diagonal elements of the pressure tensor and show that they contain the factor k_y.

Parallel-Velocity Shear

- Even for large values of parallel electron drift speed $v_{de}/v_{ti} >> 1$, ion-acoustic waves are strongly ion-Landau damped in homogeneous, isothermal plasma consisting of electrons and positively charged ions.
- For inhomogeneous plasma, the frequency depends on parallel-velocity shear. For homogeneous parallel ion flow, σ is unity, and the homogeneous ion-acoustic dispersion relation is recovered.
- D'Angelo's instability corresponds to $\sigma^2 < 0$. Shear-modified ion-acoustic waves are associated with $\sigma^2 > 0$, having real frequency and parallel wave-phase speed σc_s.
- For higher frequency, the $n>0$ ion-cyclotron resonance, along with the $n=0$ Landau resonance, must be included in evaluating the wave-particle interaction [*Lakhina*, 1987; *Gavrishchaka et al*., 2000].
- It is possible for the factor containing shear to become negative, in which case ion-cyclotron growth contributes to the overall growth of the ion-cyclotron waves.

WVU Q Machine

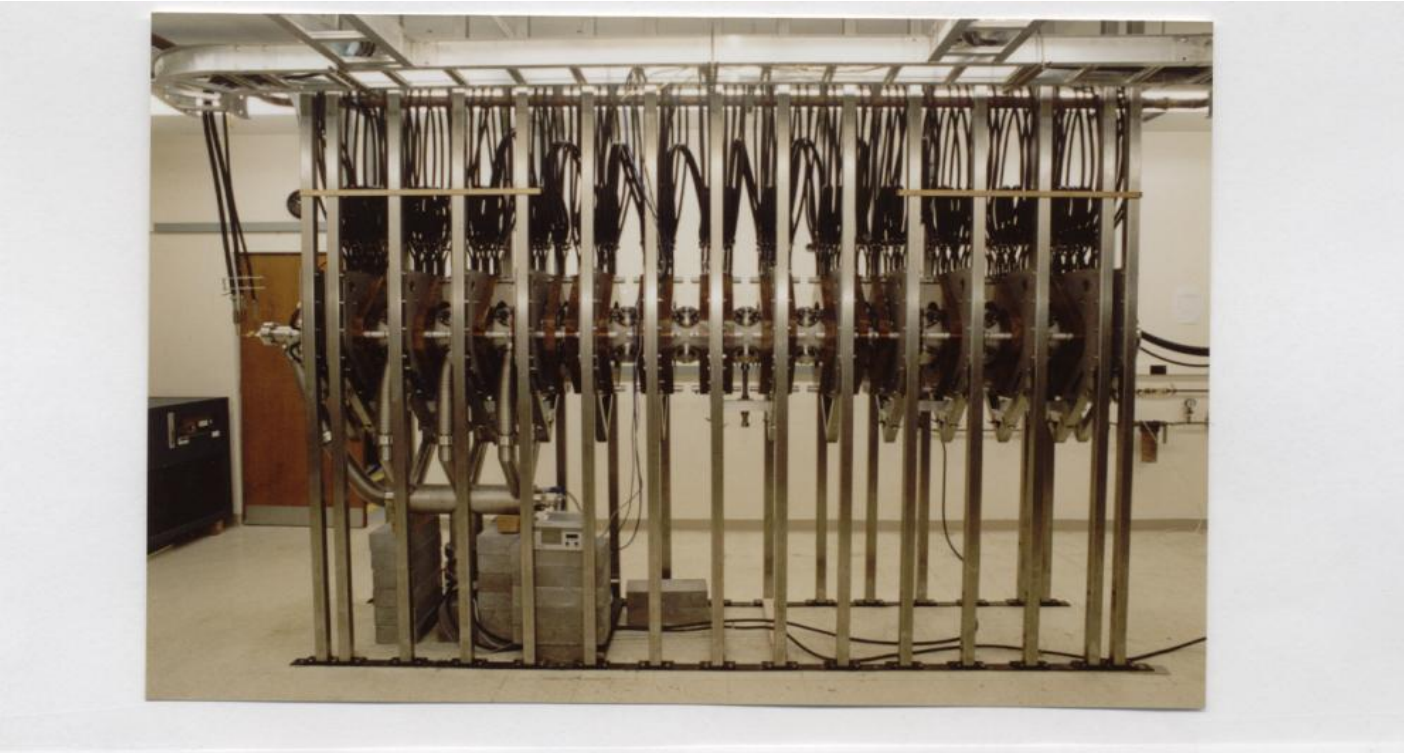

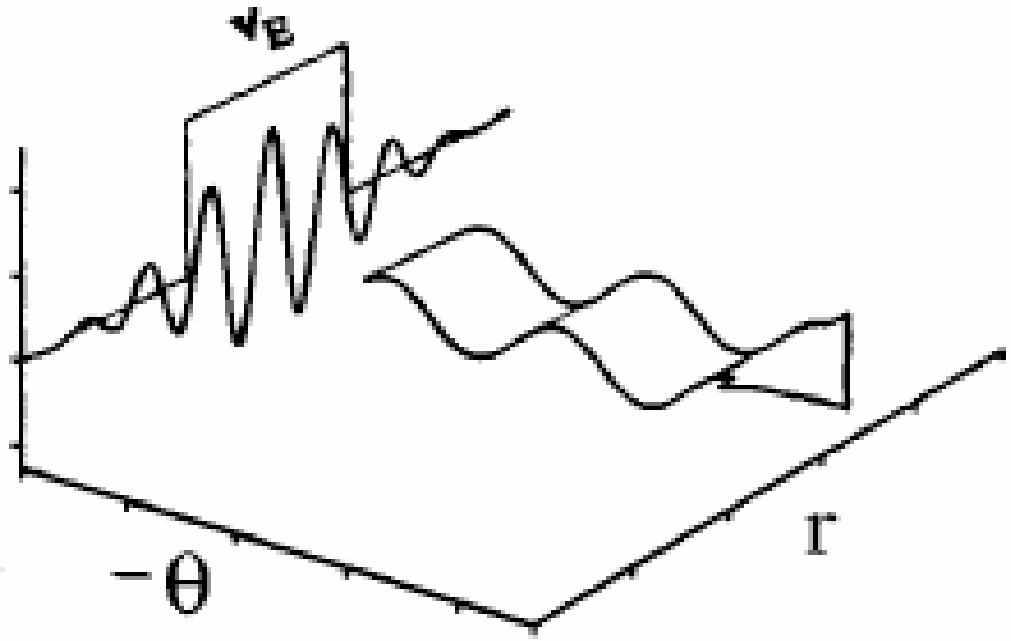

FIG. 1. Pictoral depiction of a single radial eigenmode of the IEDD instability. The "top-hat" profile of transverse flow, with maximum value v_E, is centered at nonzero radius. The IEDD waves propagate in the $\mathbf{E}\times\mathbf{B}$ direction (i.e., the $-\theta$ direction).

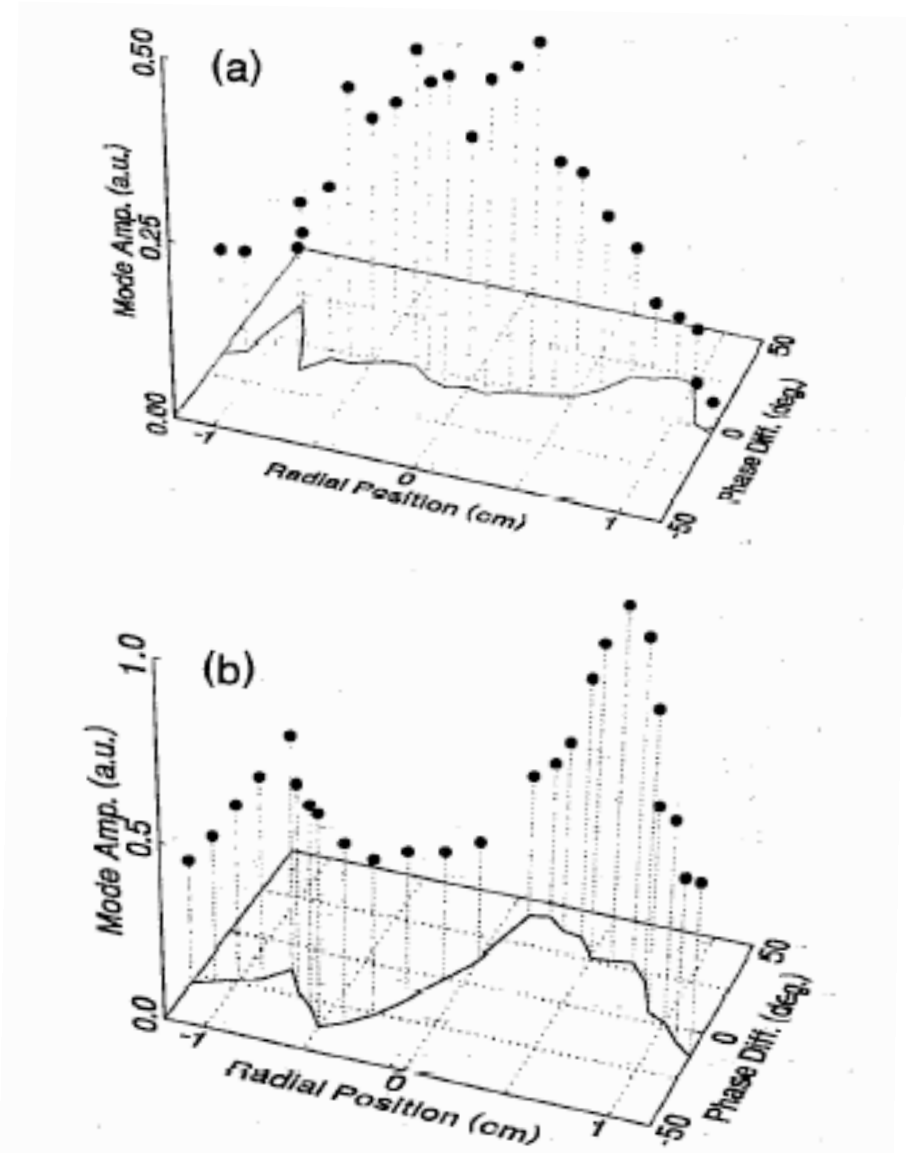

FIG. 11. Mode amplitude and relative phase versus the radius. Here (V_a, V_b) combinations are (a) (40 V, 40 V), CDEIC waves present, and (b) (14 V, −6 V), IEDD waves present. Probes are separated by 3 mm. Location of disk-electrode segments are indicated along position axis. Note that, in (b), amplitude maximum is located off-axis where shear is maximum.

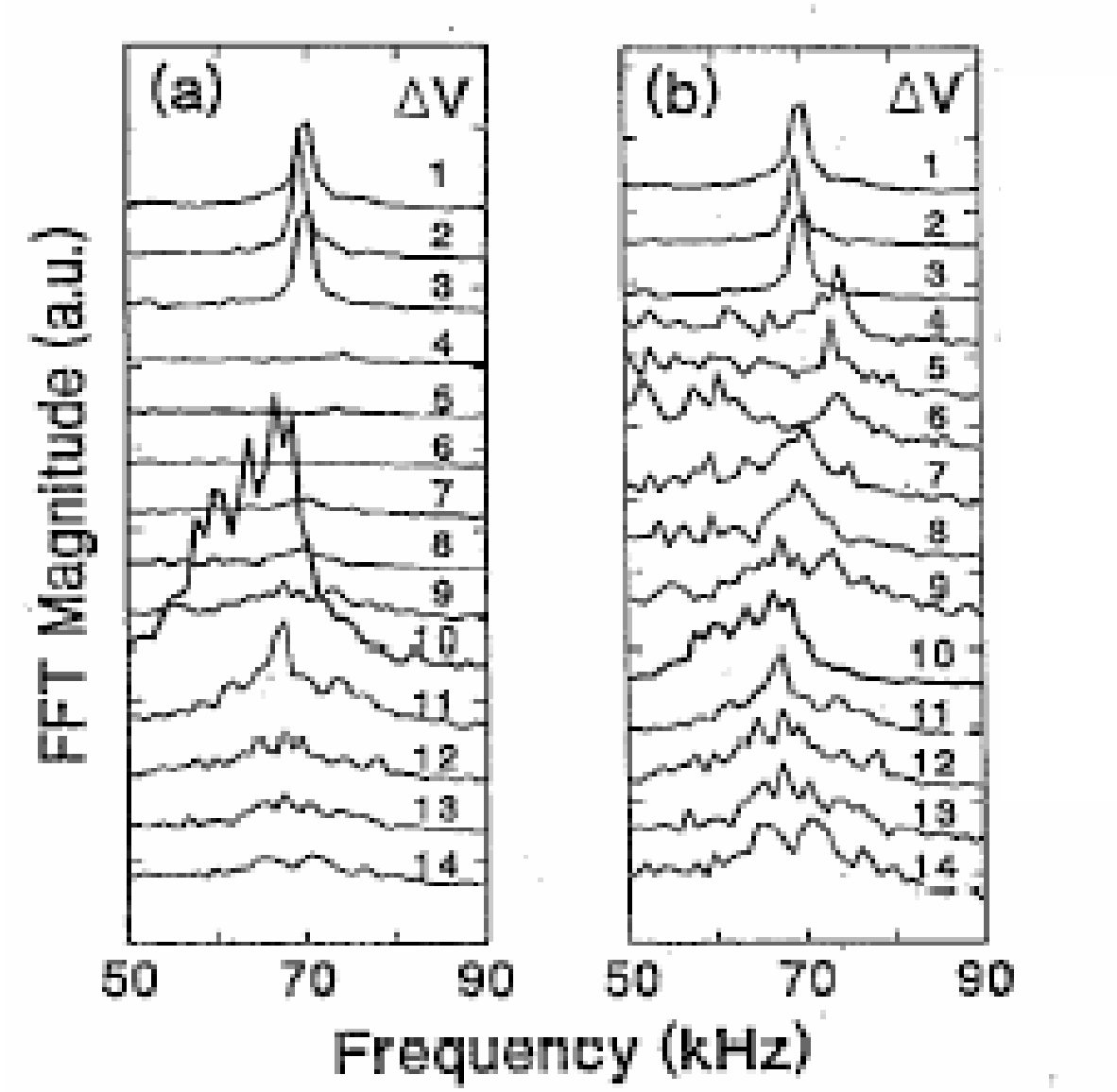
(a)
ΔV
1
2
3
4
5
6
7
8
9
10
11
12
13
14
(b)
ΔV
1
2
3
4
5
6
7
8
9
10
11
12
13
14
FFT Magnitude (a.u.)
50
70
90
50
70
90
Frequency (kHz)

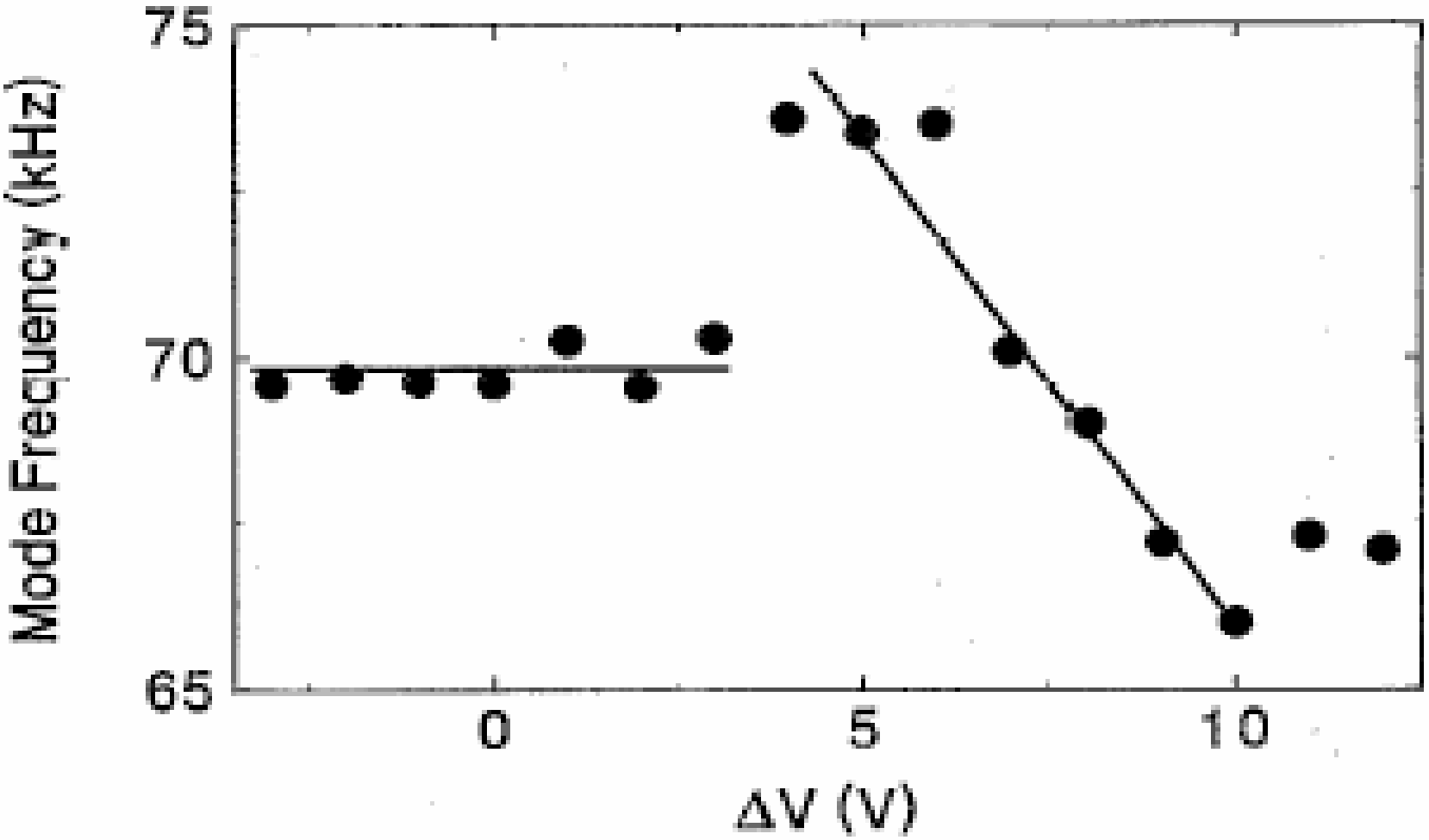
75
70
65
Mode Frequency (kHz)
0
5
10
ΔV (V)

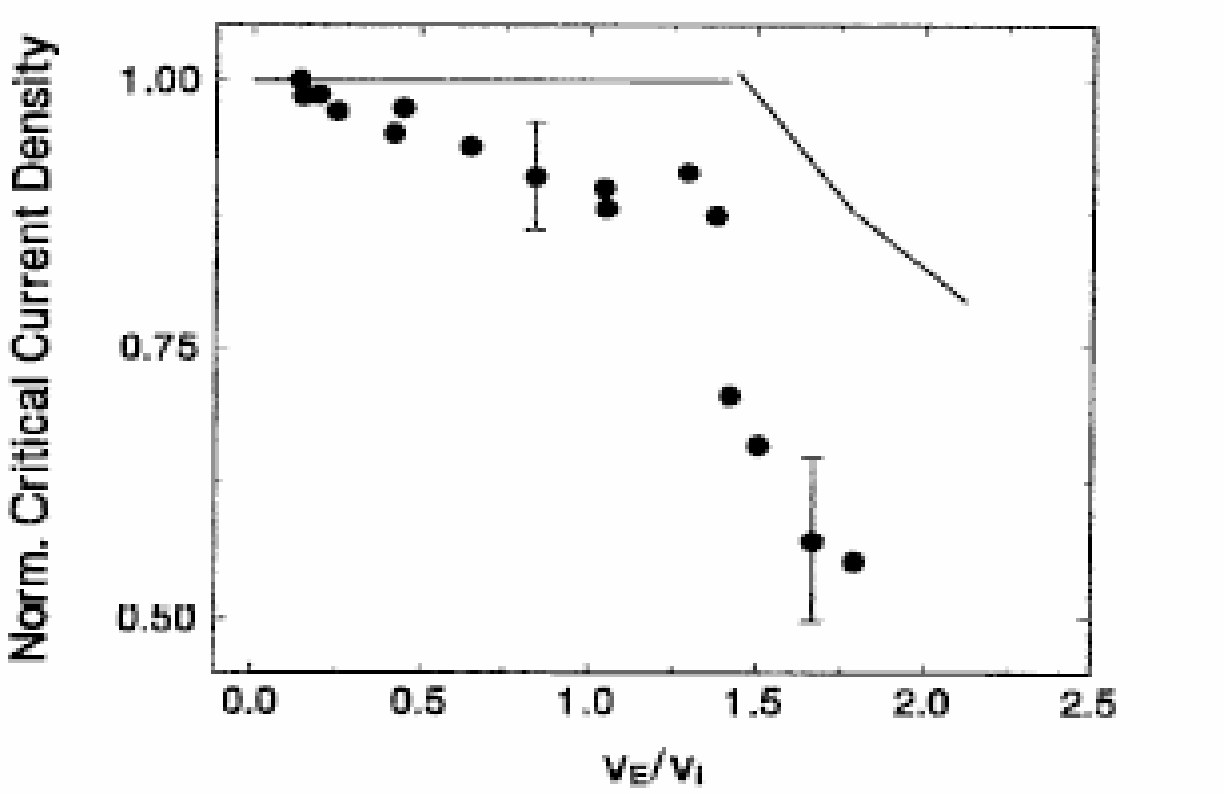

FIG. 9. The threshold value of current density as a function of localized, transverse electric field strength. Current densities are normalized to the zero-field value (refer to Ref. 15 for the details of measurement). The theoretically predicted threshold value of parallel current density normalized to the zero-field value as a function of v_E/v_i. Here $\epsilon=0.35$, $T_i/T_e=1$, and $m_i/m_e=71\ 979$. For the straight line (CDEIC instability), $(k_r\rho_i)^2=0.23$ and $(k_\theta\rho_i)^2=0$, and for the curve (IEDD instability), $(k_\theta\rho_i)^2=0.15$.

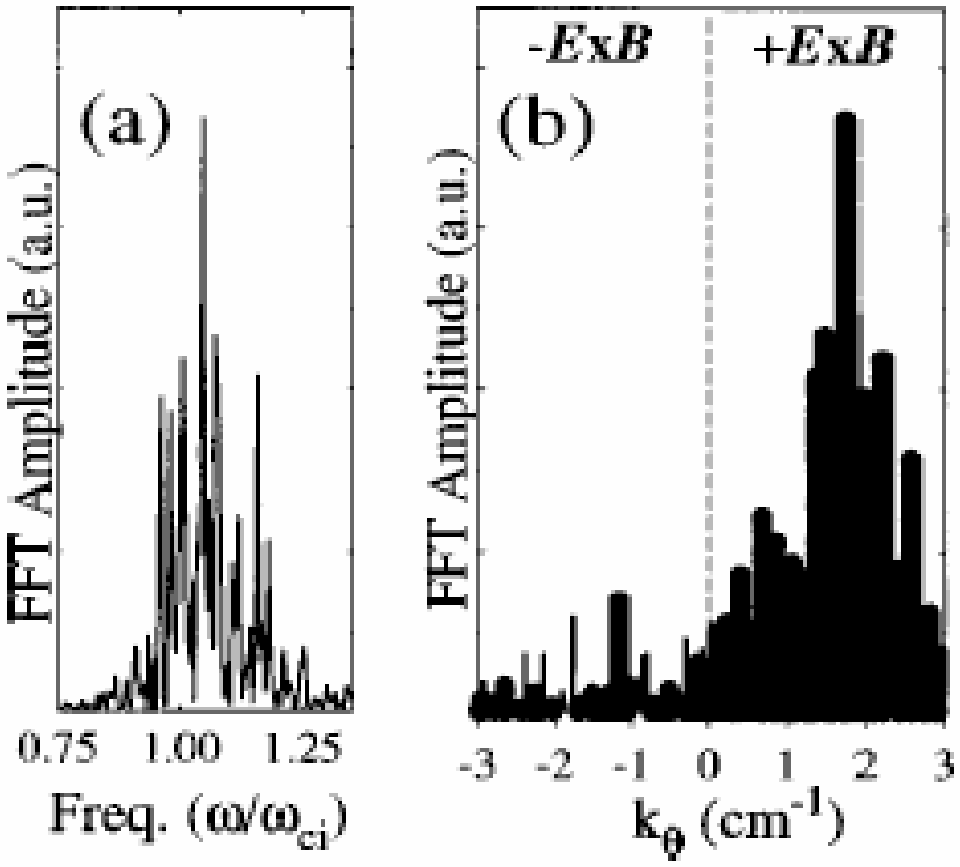

FIG. 10. IEDD waves have broad (a) frequency and (b) k_θ spectra: $V_0 = 30$ V and $V_1 = 20$ V. The six most prominent features in the frequency spectrum form a slightly spread grouping in the k_θ spectrum associated with $m = 1$.

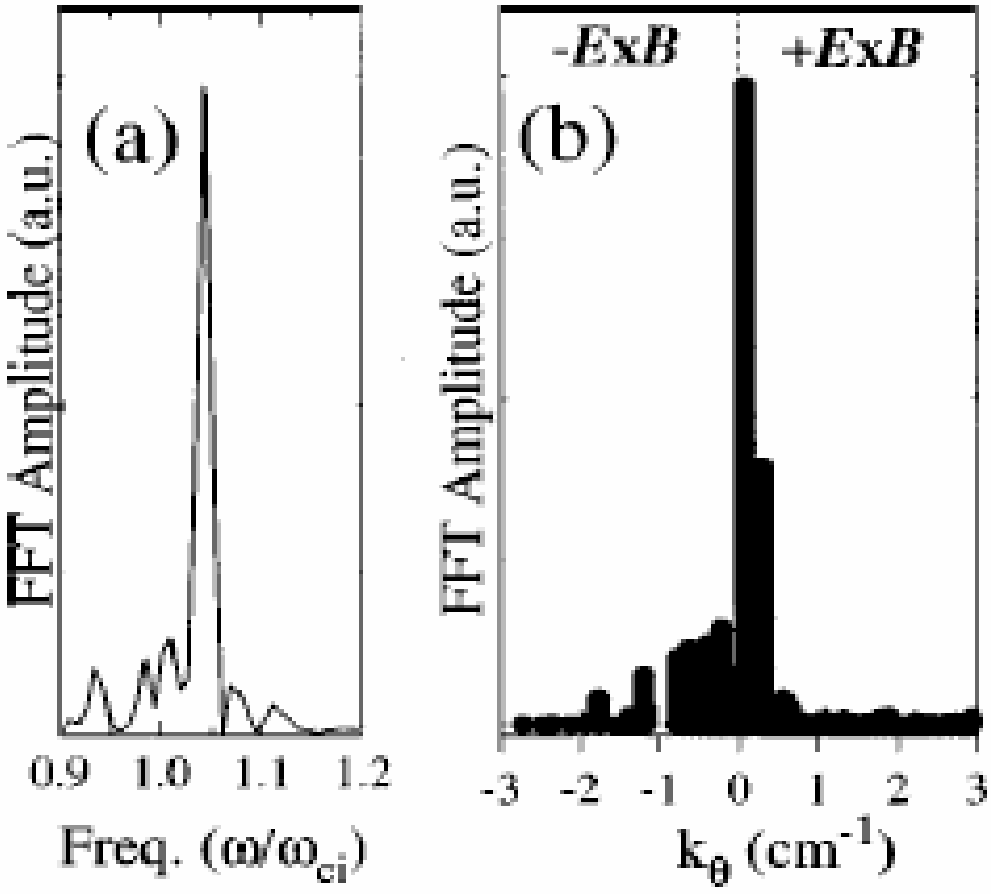

FIG. 11. CDEIC waves have narrow (a) frequency and (b) k_θ: $V_0 = 30$ V and $V_1 = 20$ V. One feature with $k_\theta = 0$ is apparent.

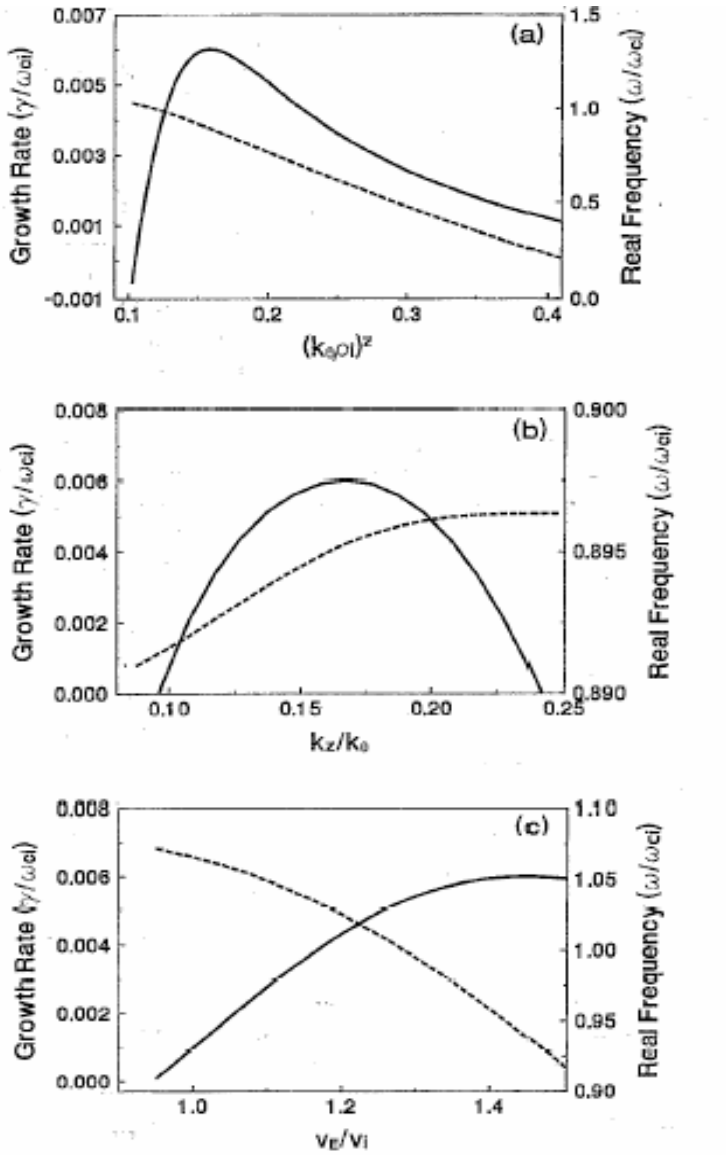

FIG. 12. Real frequency and growth rates from the general eigenvalue condition as a function of (a) $(k_y\rho_i)^2$, where $k_z/k_\theta=0.1675$, and $\nu_E/\nu_i=1.5$; (b) k_z/k_θ, where $(k_y\rho_i)^2=0.1575$, and $\nu_E/\nu_i=1.5$; and (c) ν_E/ν_i, where $(k_y\rho_i)^2=0.15$, and k_z/k_θ is adjusted within the range 0.1 to 0.2, so that γ is maximum. Here, $m_i/m_e=71\ 979$, $T_i/T_e=1$, and $\nu_e/\nu_i=30$. The relevant range of the experimental parameters are $(k_y\rho_i)^2=0.13\pm0.03$, $k_z/k_y=0.10\pm0.06$, $1<\nu_E/\nu_i\lesssim2$, and $0.9<\omega/\omega_{ci}<1.3$.

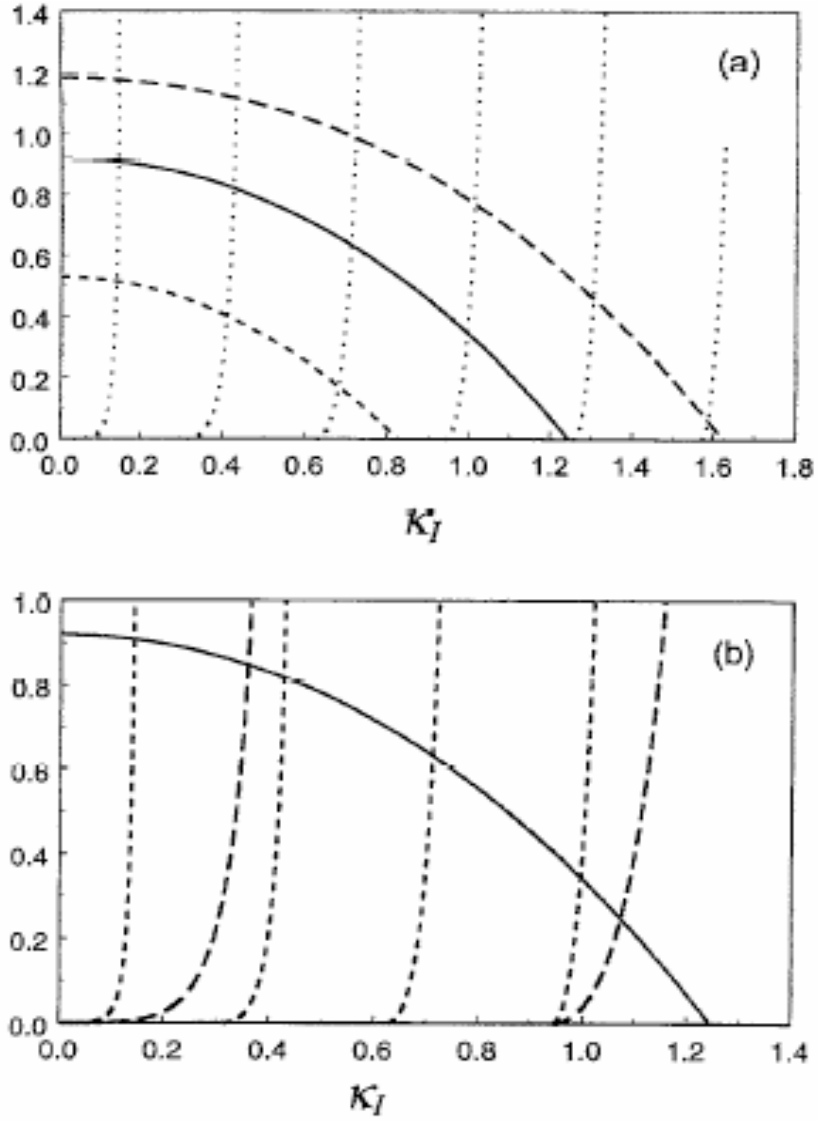

FIG. 4. Intersections of Y_1 (left-hand side of nonlocal dispersion relation) versus κ_1 (vertical lines) and Y_2 (right-hand side of nonlocal dispersion relation) versus κ_1 (quarter circles) give the roots. In (a) ν_E is varied while ϵ=0.05 is fixed: 1.5 (outer quarter circle), 1.0 (middle quarter circle), 0.5 (inner quarter circle). In (b) ϵ is varied while ν_E/ν_i is fixed: 0.05 (four vertical lines), 0.15 (two vertical lines).

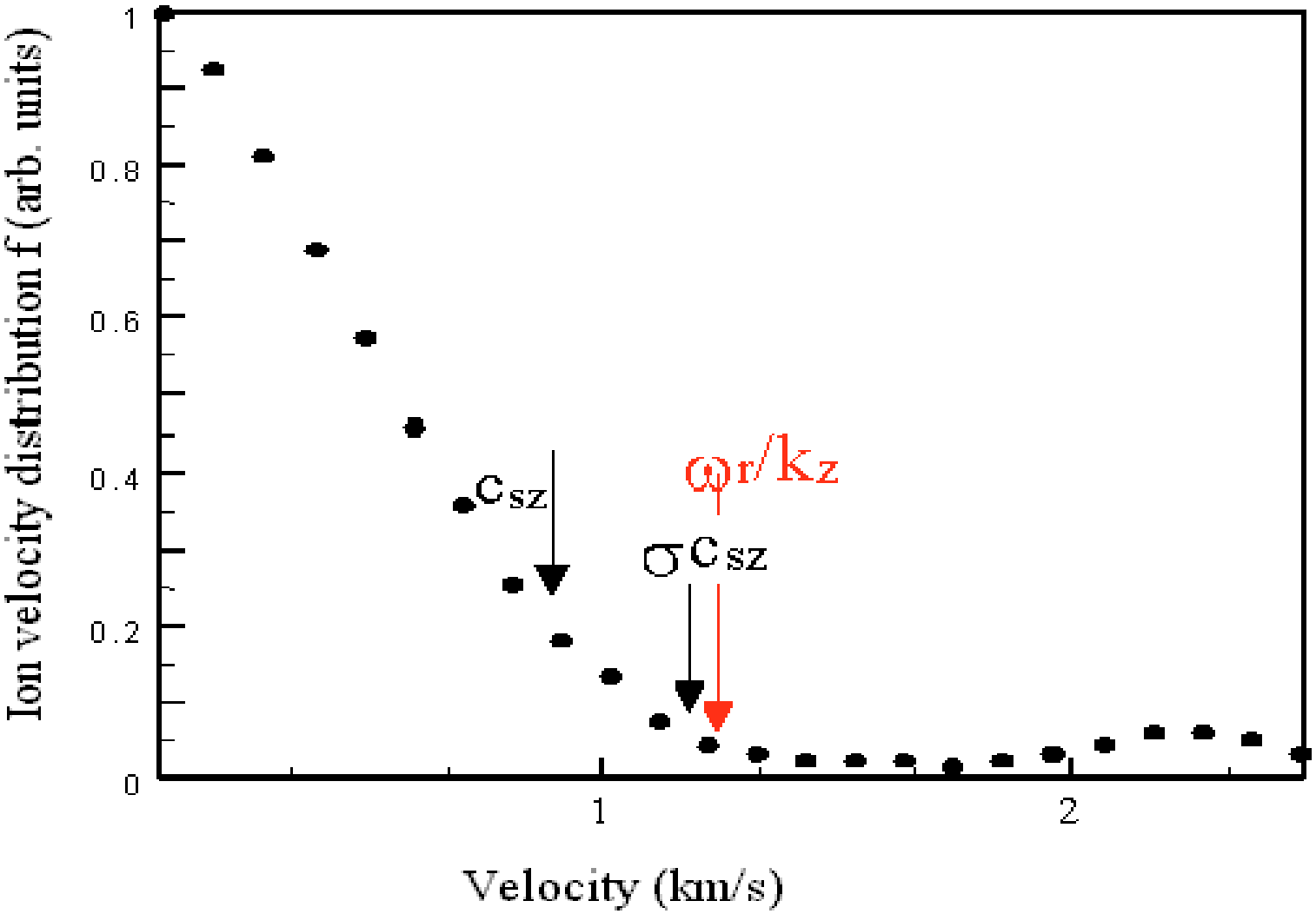
Ion velocity distribution f (arb. units)
1
0.8
0.6
0.4
0.2
0
1
2
Velocity (km/s)
csz
σcsz
ωr/kz